Efficacy and Safety of a Novel Fusogenic Oncolytic Herpes Simplex Virus

Undergraduate Research Thesis

Presented in partial fulfillment of the requirements for graduation
with honors research distinction in Biochemistry in the undergraduate colleges of The Ohio State University

by

Grace Sullivan

The Ohio State University
April 2023

Faculty Advisor: Dr. Jane Jackman, Department of Chemistry and Biochemistry
Project Advisor: Dr. Timothy Cripe, Department of Pediatrics

Acknowledgements

I want to recognize Pin-Yi Wang, Julia Halley, Domenica Marino, Kevin Cassady, and Timothy Cripe as co-authors of this work. I specifically want to thank Dr. Pin-Yi Wang for her mentorship, support, and patience over the past three years. She has made me into the scientist I am today, and I am grateful she has instilled a sense of independence and confidence in me to answer scientific questions. We encountered a lot of failures and setbacks over the past three years, but I will forever cherish sharing the feelings of progress and success with her.

I want to thank Dr. Timothy Cripe for welcoming me into his lab and continuously supporting me. I have learned so much about science by witnessing him think critically about data and provide direction to the lab, and his feedback has provided for my growth as a researcher. I hope to emulate his sense of leadership and passion for improving patient outcomes one day. I also want to thank all the other members of Cripe Lab for providing an environment conducive to learning. It has been a privilege to work with each one of you, and I have hope for a better future because of the passion and work ethic I have witnessed everyone exhibit daily. Thank you for choosing to invest in me.

I want to thank Dr. Jane Jackman and Dr. Eric Danhart for serving as faculty members on my defense committee and shaping my undergraduate education in biochemistry.

Finally, I want to thank my family, and specifically my parents, Andrea and Scott. Their unwavering support has allowed me to grow into the person I am today. Because of their encouragement and love, I can chase after my dreams. Thank you for providing such a firm foundation on which I can build my life.

This work was supported by CancerFree Kids, the Elsa U. Pardee Foundation, R21CA223104-02, and the 2022-2023 Undergraduate Research Scholarship.

Table of Contents

Introduction

Although impressive strides have been made in increasing survival rates for numerous pediatric cancers, pediatric cancer remains the leading cause of childhood death by disease (Cunningham et al., 2018). Responsible for 30% of all pediatric cancers, solid tumors are a heterogeneous group of cancers that include but are not limited to neuroblastoma, rhabdomyosarcoma, and Ewing's sarcoma (Kline & Sevier, 2003). The standard of care for pediatric patients diagnosed with solid tumors includes surgical resection, chemotherapy, and radiation (Kline & Sevier, 2003). Despite multimodal treatment approaches, patients diagnosed with solid tumors have poor long-term survival rates (Cripe et al., 2015). Because of their prevalence and poor prognoses, it is imperative to develop therapeutics to treat solid tumors specifically.

Proper targeting of therapeutics is of paramount importance to minimize off-target effects and mitigate potential harm, especially when developing treatments for children to reduce the long-term burden of a cancer diagnosis. In this way, oncolytic herpes simplex viruses (oHSV) are promising therapeutics for pediatric solid tumors because they can be engineered to replicate theoretically only in cancer cells.

Herpes simplex virus is a double-stranded DNA virus with a 152 kilobase pair genome that contains roughly 80 genes (Roizman et al., 2013). HSV-1 can enter human cells through different receptors, namely nectin-1, herpes virus entry mediator (HVEM), and 3-O-sulfated HS (Agelidis & Shukla, 2015). Upon entry, HSV-1 is transported to the nucleus, where transcription and replication begin (Kukhanova et al., 2014). Host RNA-polymerase II transcribes the viral genome into viral mRNA, which is translated into viral proteins that modulate the expression of immediate early, early, and late genes (Kukhanova et al., 2014). Immediate early genes such as ICP0, ICP4,

ICP22, ICP27, and ICP47 are involved in "disabling certain innate and adaptive immune functions" and facilitating the replication of the viral genome through regulation (Peters & Rabkin, 2015). Early genes encode proteins essential for viral replication such as UL30 (DNA polymerase), ICP8 (single-strand DNA-binding protein), and UL9 (origin binding protein) (Weller & Coen, 2012). After the viral genome is replicated, the late genes that encode the structural proteins of HSV-1 are expressed, enabling virion packaging (Lehman & Boehmer, 1999). The production of virions provides for cell lysis and thereby spread of HSV-1 (Peters & Rabkin, 2015).

About 20% of the HSV-1 genome, though, encodes "nonessential genes" (Varghese & Rabkin, 2002). As a large virus, these nonessential regions are unique to HSV-1 when compared to small viruses (Peters & Rabkin, 2015). Researchers can modify these nonessential regions to engineer oncolytic HSVs that still replicate, making HSV-1 a good platform for oncolytic virotherapy. Furthermore, if widespread HSV-1 infection occurred, anti-herpetic medications can be used to mitigate side effects of oncolytic virotherapy (Nguyen & Saha, 2021). However, since HSV-1 is widely prevalent among the population, patients can have neutralizing antibodies specific to HSV, which can limit the efficacy of oHSVs (Xu et al., 2002; Groeneveldt et al., 2023). Nonetheless, oHSVs have demonstrated preclinical and clinical antitumor efficacy, and currently one oHSV, Imlygic®, is FDA-approved (Bilsland et al., 2016).

One prevailing problem in the oHSV discipline is achieving a potency that results in oncolysis and a clinically significant reduction in tumor burden and improvement in patient survival while also maintaining safety (Kuhn et al., 2008). To address this problem, Dr. Wang, a senior scientist in Dr. Timothy Cripe's laboratory, utilized the directed evolution strategy to engineer a potent virus through genotypic recombination. Over the course of a year, Dr. Wang serially passaged oHSV-resistant cells infected with both 17TermA and rRp450. Over time,

through directed evolution, genetic information was exchanged between the two parent viruses to enable viral entry into the resistant cells. The resulting virus was purified and sequenced. The new virus, hereafter referred to as Mut-3, contained five nonsynonymous mutations compared to both parents (sequencing not shown; **Figure 1A**). Mut-3 is a highly potent, wild type-like oHSV, so for safety reasons, attenuation was required.

While wild type oHSVs exist, oHSVs are attenuated through various mechanisms to ensure both safety and proper targeting of the oHSV to the tumor as opposed to healthy tissues. UL39 is a locus located within the unique long (UL) region of oHSV. UL39 encodes infected cell protein 6 (ICP6), which is the large subunit of viral ribonucleotide reductase (Nguyen et al., 2020). Ribonucleotide reductase catalyzes the reduction of the 2' hydroxyl group of ribose, the sugar involved in ribonucleotides, to form deoxyribonucleotides, which are the building blocks of DNA. As oHSV is a double-stranded DNA virus, to replicate, sufficient levels of deoxyribonucleotides must be present in the cell to replicate the viral genome. In deleting UL39, the oHSV lacks the genetic template that infected cell machinery will transcribe and later translate into viral ribonucleotide reductase. Therefore, for an oHSV to replicate, it will rely on the cell's ribonucleotide reductase to convert ribonucleotides to deoxyribonucleotides. In healthy, non-dividing cells, basal levels of ribonucleotide reductase are not high enough to facilitate efficient replication of oHSV because there is not sufficient conversion of ribonucleotides to deoxyribonucleotides, which are needed for replication of the oHSV viral genome composed of DNA (Nguyen et al., 2020). However, in cancer cells, because cancer cells are rapidly dividing, the basal levels of ribonucleotide reductase are elevated compared to healthy cells to ensure there are sufficient pools of deoxyribonucleotides to replicate the cell's genome during the cell division process. Consequently, the ribonucleotide reductase present in cancer cells can compensate for the

lack of viral ribonucleotide reductase coming from the oHSV, and the oHSV is replicated because there are deoxyribonucleotide pools from which cell machinery can effectively steal. By this mechanism, an oHSV can be effectively targeted towards cancer cells.

KOS is a wild-type strain of HSV-1. 17TermA is another oHSV with a 17^+ backbone, but it contains a deletion of RL1, the gene that encodes infected cell protein 34.5 (ICP34.5), which is a neurovirulence factor (Bolovan et al., 1994). In deleting RL1, attenuation is achieved because the neurovirulence factor is not transcribed and translated, so replication and therefore spread is limited. rRp450 has a KOS backbone, but it contains a deletion of UL39, the gene that encodes ICP6. In place of UL39, CYP2B1, the rat gene for cytochrome p450 that facilitates the bioactivation of cyclophosphamide, leading to cytotoxicity, is inserted (Chase et al., 1998).

17TermA and rRp450 are the parent viruses that, through directed evolution, underwent genotypic recombination that generated Mut-3, a highly potent oHSV **(Figure 1A)**. Mut-3 contains nonsynonymous mutations from both parent viruses (not shown). Mut-3 was attenuated by deleting the UL39 locus that encodes ICP6 and inserting GFP in its place using the CRISPR/Cas9 gene editing system **(Figure 1A)**. rRp450 serves as a fusogenic control to Mut-3Δ6, whereas A7H3 serves as a non-fusogenic control to both rRp450 and Mut-3Δ6.

Fusogenic viruses facilitate the spread of virus through cell-to-cell contact and fusion, resulting in the formation of syncytia (Krabbe & Altomonte, 2018). As surrounding cells are fused together, virion can pass into new cells and infect them, eventually resulting in tumor lysis. Consequently, fusogenic viruses have characteristically large plaques that are often circular but can be oddly shaped. Fusogenic viruses are of interest in treating cancer because of their ability to spread within the tumor, thereby facilitating oncolysis (Krabbe & Altomonte, 2018). Non-

fusogenic viruses, on the other hand, do not promote virus spread through syncytia formation, and they have characteristically small, circular plaques (Ennis, et al., 2009).

Mut-3Δ6 exhibits a gigantic fusogenic plaque phenotype **(Figure 1C)**. Because of the massive plaque size of Mut-3Δ6, it was hypothesized that Mut-3Δ6 has the potential to outperform other oHSVs in treating solid tumors. Consequently, Mut-3Δ6 was characterized for its *in vitro* safety, *in vitro* cytotoxicity, *in vivo* safety, and *in vivo* anti-tumor efficacy to evaluate its potential as a cancer therapeutic.

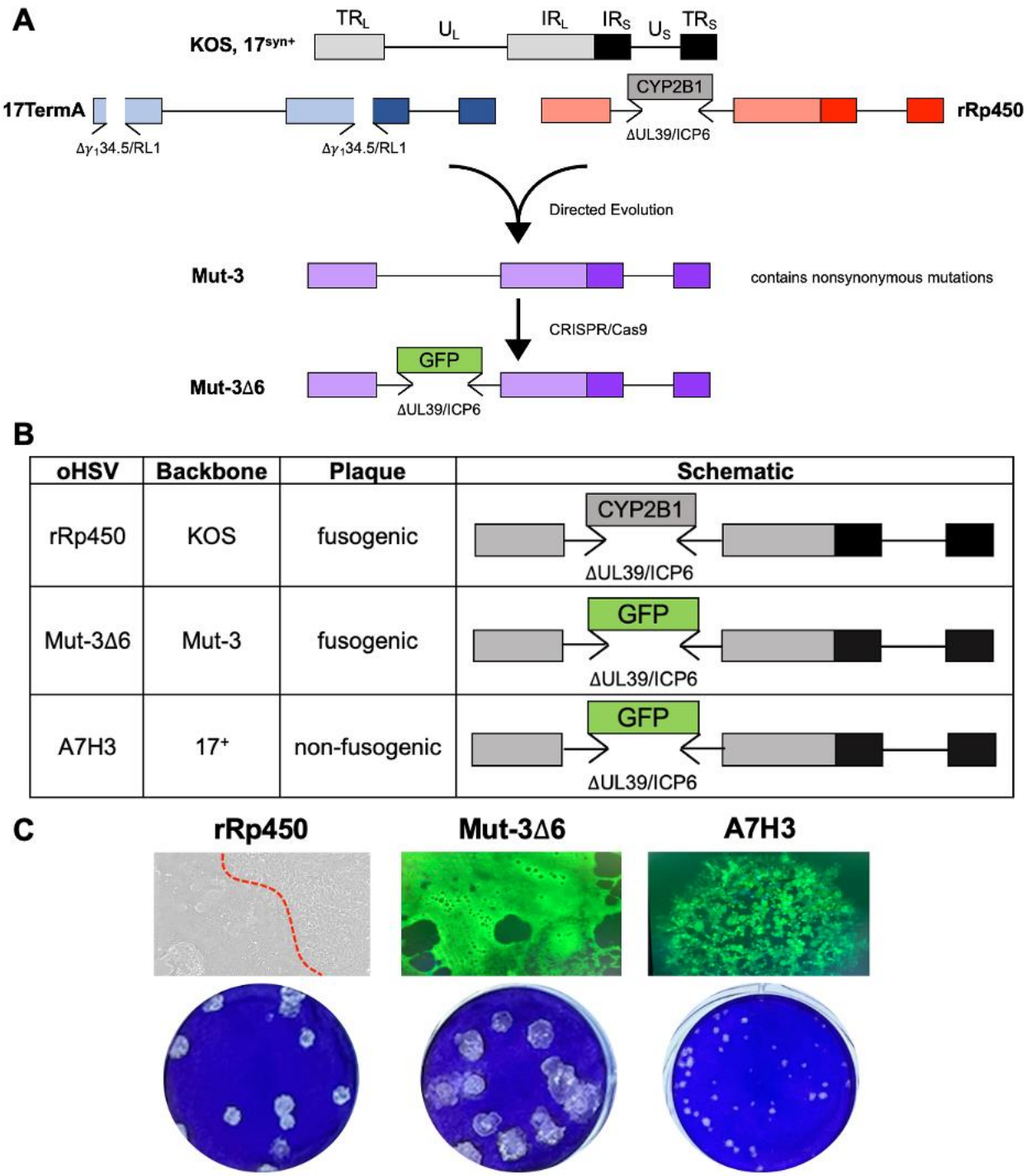

Figure 1: Mut-3Δ6 exhibits a gigantic fusogenic plaque phenotype. A. Schematic depicting the directed evolution strategy used to generate Mut-3 and the attenuation strategy to generate Mut-3Δ6. B. Table characterizing each oHSV investigated. C. Phase and green filter images of Vero cells infected with rRp450, Mut-3Δ6, or A7H3 (top row), and Vero cells stained with crystal violet after oHSV infection (bottom row).

Preliminary Results

The attenuation of Mut-3Δ6 was confirmed by *in vitro* MTS cytotoxicity assays by Julia Halley, a former member of Cripe Lab **(Figure 2)**. In differentiated human foreskin keratinocytes, there was a significant difference in the survival of cells infected with Mut-3Δ6 and cells infected with Mut-3, with Mut-3Δ6 cells surviving significantly more. Differentiated human foreskin keratinocytes serve as a model of normal, healthy cells that no longer undergo cell division. The reduced potency of Mut-3Δ6 in differentiated keratinocytes indicated Mut-3Δ6 was successfully attenuated and demonstrated a significantly reduced potency in differentiated cells. This reduced potency in differentiated keratinocytes, which are analogous to healthy cells, indicated Mut-3Δ6 is safe *in vitro*. In undifferentiated human foreskin keratinocytes, there was no significant difference between the survival of cells infected with Mut-3 (unattenuated and highly potent) and cells infected with Mut-3Δ6. Undifferentiated human foreskin keratinocytes undergo cell division. The potency of Mut-3Δ6 was comparable to the potency of unattenuated Mut-3 in undifferentiated keratinocytes, indicating the potential of Mut-3Δ6 as a potent cancer therapeutic.

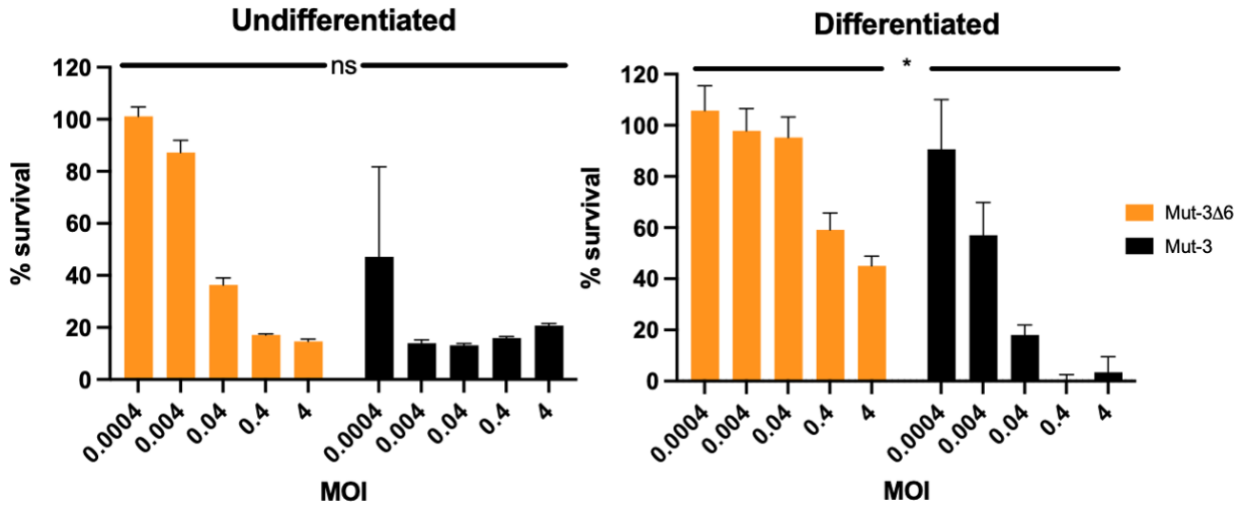

Figure 2: Mut-3Δ6 is safe *in vitro*. Mut-3Δ6 demonstrated *in vitro* safety in differentiated human foreskin keratinocytes (four days post viral infection) while retaining its potency in undifferentiated human foreskin keratinocytes (three days post viral infection). *: p = 0.0107.

Having established the *in vitro* safety of Mut-3Δ6, Dr. Pin-Yi Wang conducted an *in vivo* toxicology study to determine if Mut-3Δ6 was safe *in vivo*. Immunocompetent Balb/c mice of both sexes were intravenously injected with 1e8 pfu (plaque forming units) Mut-3Δ6 or 1e5 pfu, 1e6 pfu, or 1e7 pfu KOS and monitored for signs of morbidity. To analyze the biodistribution of Mut-3Δ6, mice injected with Mut-3Δ6 were designated to be sacrificed at a specific timepoint after virus injection: 24 hours, 14 days, 28 days, 54 days, or 85 days. None of the mice injected with Mut-3Δ6 were sacrificed before the designated timepoint due to animal health concerns (**Figure 3B**), indicating Mut-3Δ6 was well-tolerated in immunocompetent mice. Mice injected with 1e6 pfu or 1e7 pfu KOS quickly deteriorated, and all were sacrificed within a week after virus injection. However, the 1e5 pfu KOS injection was not lethal to the Balb/c mice (**Figure 3C**). There was a significant difference in survival of mice injected with 1e6 pfu KOS versus mice injected with 1e8 pfu Mut-3Δ6 ($p = 0.0002$). Also, there was a significant difference in survival of mice injected with 1e7 pfu KOS versus mice injected with 1e8 pfu Mut-3Δ6 ($p = 0.0003$).

When a mouse was sacrificed, their brain, heart, kidney, liver, lung, spleen, and testes (male) or ovaries (female) were harvested and ground into tissue powder. Domenica Marino, a former member of Cripe Lab, evaluated the biodistribution of KOS by performing powder plaque assays. KOS was detected in the brain, kidneys, and ovaries of sick female mice injected with 1e6 pfu or 1e7 pfu KOS (**Figure 3D**). I assisted Domenica Marino in performing the powder plaque assays to evaluate the biodistribution of Mut-3Δ6. Mut-3Δ6 was only detected in organs harvested 24 hours post virus injection in male and female mice. In both genders, Mut-3Δ6 was notably detected in the heart and kidneys at 24 hours. Mut-3Δ6 was cleared from all

organs in male and female immunocompetent mice 14 days after injection (**Figure 3E**). This survival and biodistribution data indicate Mut-3Δ6 is safe *in vivo.*

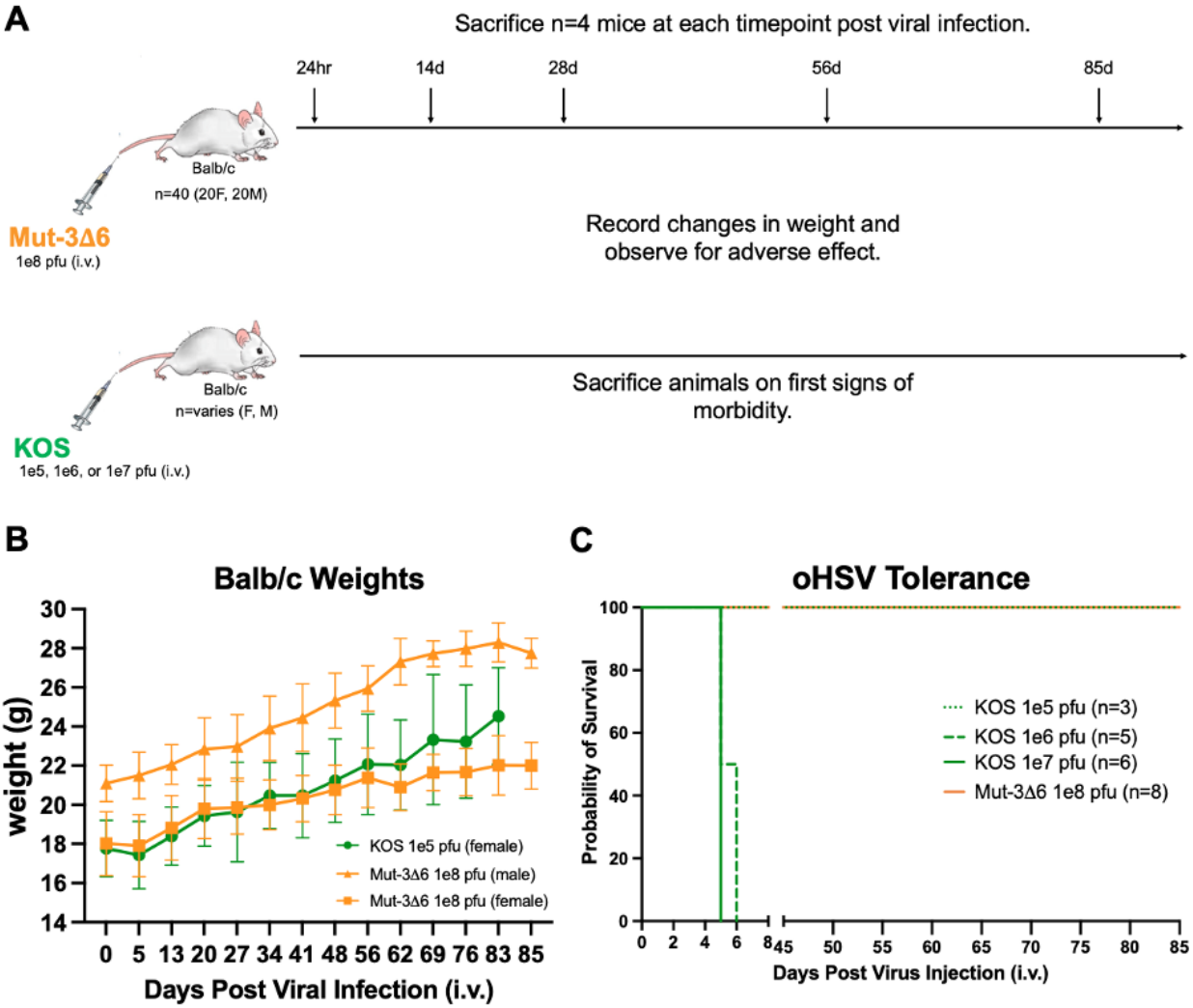

D

Dose	Brain	Heart	Kidney	Liver	Lung	Ovary	Spleen
1e6 pfu	2/3	-	3/3	-	-	2/2	-
1e7 pfu	3/3	-	2/3	-	-	3/3	-

E

	24hr		14d	28d	56d	85d
	Male	Female				
Brain	0/4	2/4	-	-	-	-
Heart	2/4	3/4	-	-	-	-
Kidney	2/4	4/4	-	-	-	-
Liver	1/4	2/4	-	-	-	-
Lung	1/4	0/4	-	-	-	-
Spleen	1/4	0/4	-	-	-	-
Testes/Ovaries	1/4	3/4	-	-	-	-

Figure 3: Mut-3Δ6 has demonstrated *in vivo* safety. A. *In vivo* toxicology study design in

Balb/c mice. B. Mice injected with 1e8 pfu Mut-3Δ6 did not lose weight after injection. C. Mut-3Δ6 was well-tolerated *in vivo*, as no mice died during the study duration (1e6 pfu KOS vs. Mut-3Δ6: $p = 0.0002$; 1e7 pfu KOS vs. Mut-3Δ6: $p = 0.0003$). D. KOS was detected in the brain, kidneys, and ovaries of female mice injected with 1e6 pfu or 1e7 pfu KOS that were sacrificed due to signs of morbidity. E. Mut-3Δ6 was only detected in organs harvested 24 hours post virus injection, and Mut-3Δ6 was cleared from all organs in male and female immunocompetent mice 14 days after injection. -: not detected by powder plaque assay.

Results

The *in vitro* cytotoxicity of novel fusogenic oHSV Mut-3Δ6 was investigated through MTS cytotoxicity assays. Numerous cell lines were screened, and the *in vitro* cytotoxicity data is summarized in **Table 1**. Cytotoxicity data for cell lines that were selected for further investigation is discussed below. MTS cytotoxicity experiments were conducted at two cell densities, low (5,000 cells/well) and high (20,000 cells/well), to potentially elucidate the fusogenic advantage of rRp450 and Mut-3Δ6 in killing cancer cells.

When Rh30 (human rhabdomyosarcoma) was seeded at a low density, at MOIs of 0.1 and 1, Mut-3Δ6 was significantly more potent than fusogenic control rRp450 and non-fusogenic control A7H3. When Rh30 was seeded at a high density, Mut-3Δ6 was significantly more potent ($p \leq 0.0001$) than rRp450 at an MOI of 0.1, as roughly 20% of Rh30 cells were alive three days after infection with Mut-3Δ6 whereas 70% of cells were alive three days after infection with rRp450 (**Figure 4**).

In SK-N-AS, a human neuroblastoma line, both fusogenic viruses (rRp450 and Mut-3Δ6) were significantly more potent than the non-fusogenic virus, A7H3, when cells were seeded at a low density. Additionally, rRp450 was significantly more potent than Mut-3Δ6 at all MOIs equal to or above 0.1. In the high-density setting, Mut-3Δ6 was significantly more potent than rRp450 ($p \leq 0.001$) and A7H3 ($p \leq 0.0001$) at MOI 0.001, and both fusogenic viruses exceeded IC_{50} at MOI 0.001. At MOIs greater than 0.001, though, rRp450 was significantly more potent than Mut-3Δ6. In the high-density setting, the fusogenic viruses were significantly more potent than the non-fusogenic virus at all MOIs tested (**Figure 4**).

CHP-134 is a human neuroblastoma line that is known to be susceptible to oHSV infection in general (Wang et al., 2015). It was hypothesized that the three oHSVs investigated

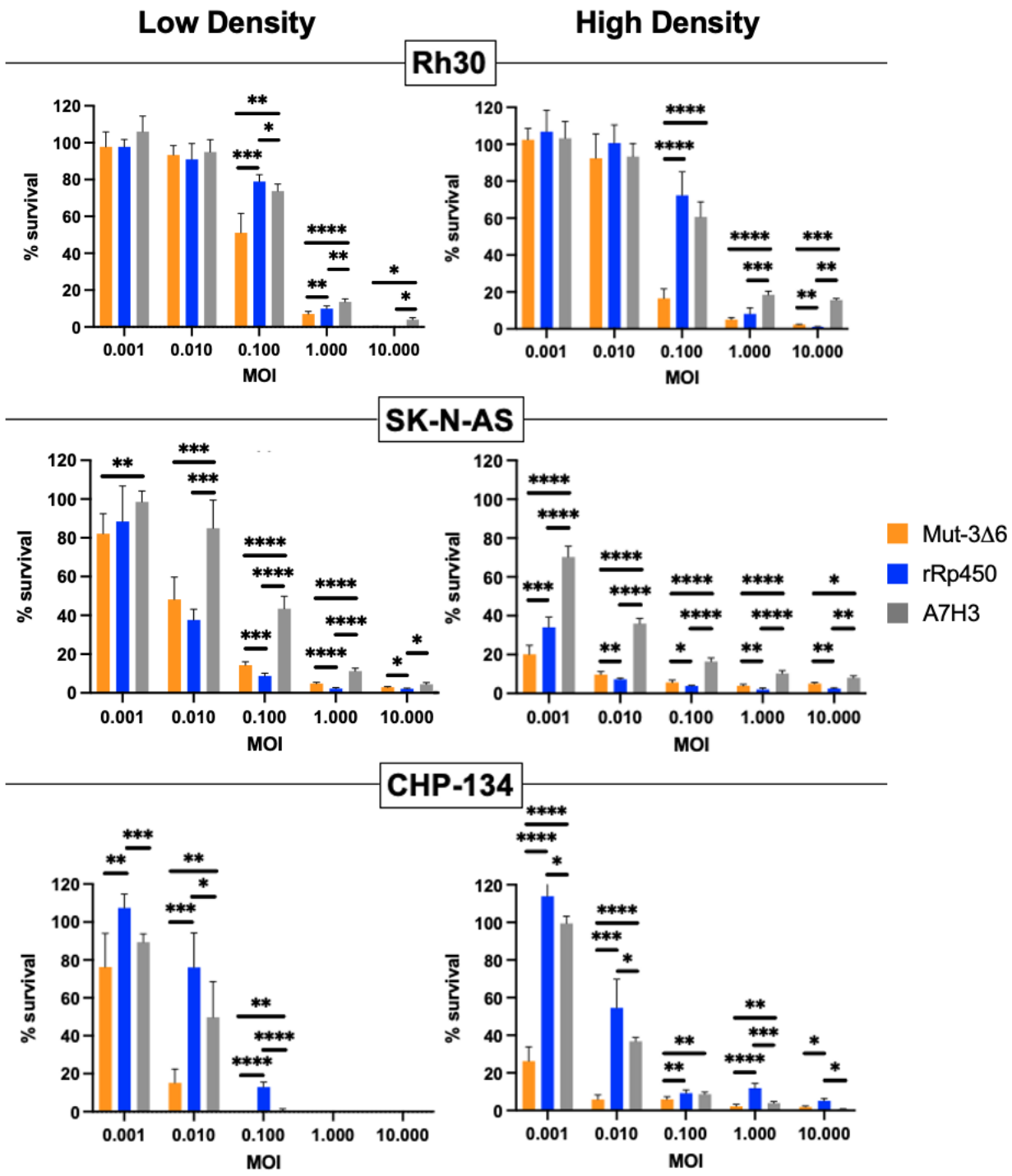

Figure 4. Mut-3Δ6 had significantly greater *in vitro* potency in Rh30, SK-N-AS, and CHP-134. Cells were seeded at low density (5,000 cells/well) and high density (20,000 cells/well) and infected the next day. Cell survival was assayed three days after oHSV infection using MTS/PMS reagent. *: $p \leq 0.05$; **: $p \leq 0.01$; ***: $p \leq 0.001$; ****: $p \leq 0.0001$

would have similar potencies due to the sensitivity of CHP-134 to oHSV infection. However, when cells were seeded at a low density, Mut-3Δ6 was significantly more potent than rRp450 at MOIs of 0.001, 0.01, and 0.1. When cells were seeded at a high density, Mut-3Δ6 exhibited significantly higher potency in CHP-134 cells compared to the other ΔICP6 viruses tested at MOIs of 0.001, 0.01, 0.1, and 1, most noticeably at MOIs of 0.001 and 0.01. Furthermore, Mut-3Δ6 exceeded IC_{50} at the lowest MOI tested, 0.001 (**Figure 4**).

		Low Density			High Density		
Tumor Type	Cell Line	Mut-3Δ6	rRp450	A7H3	Mut-3Δ6	rRp450	A7H3
RMS	Rh30	+	+	+	++	+	+
EWS	CHLA-9	-	-	-	-	-	+
	CHLA-10	++	++	++	+++	+++	+++
NBL	CHLA-20	+++	+++	++	+++	+++	+++
	CHLA-255	++	+++	++	+++	+++	+++
	SK-N-BE(2)	+++	+++	++	+++	+++	++
	CHP-134	+++	++	+++	+++	++	+++
	SK-N-AS	+++	+++	++	+++	+++	+++

Table 1: Summary of *in vitro* MTS cytotoxicity assays in which cell survival was evaluated at three days post infection at MOIs of 0.001, 0.01, 0.1, 1, and 10 in at least two independent experiments. +++ means IC_{50} occurs below MOI 0.01; ++ means IC_{50} occurs between MOI 0.01-0.1; + means IC_{50} occurs between MOI 0.1-1; - means IC_{50} occurs above MOI 1. (RMS: rhabdomyosarcoma; EWS: Ewing sarcoma; NBL: neuroblastoma).

Based on the *in vitro* cytotoxicity data, three cell lines were selected for *in vitro* viral replication assays: Rh30 (RMS), SK-N-AS (NBL), and CHP-134 (NBL). These candidate cell lines were selected because engineered oHSV Mut-3Δ6 exhibited higher potency compared to rRp450 and A7H3 and its potency occurred at low MOIs (0.001, 0.01), which is desirable because treatment regimens with lower MOIs can be translated more easily to the clinic. It was hypothesized that Mut-3Δ6 replicates more than rRp450 and A7H3, and this higher replication of Mut-3Δ6 explains its enhanced potency.

In SK-N-AS, rRp450 replicated significantly more than A7H3 two hours after infection, but 24 hours after infection, Mut-3Δ6 replicated significantly more than rRp450 and A7H3. After 48 hours, Mut-3Δ6 replicated comparably to rRp450. At 72 hours, there were no

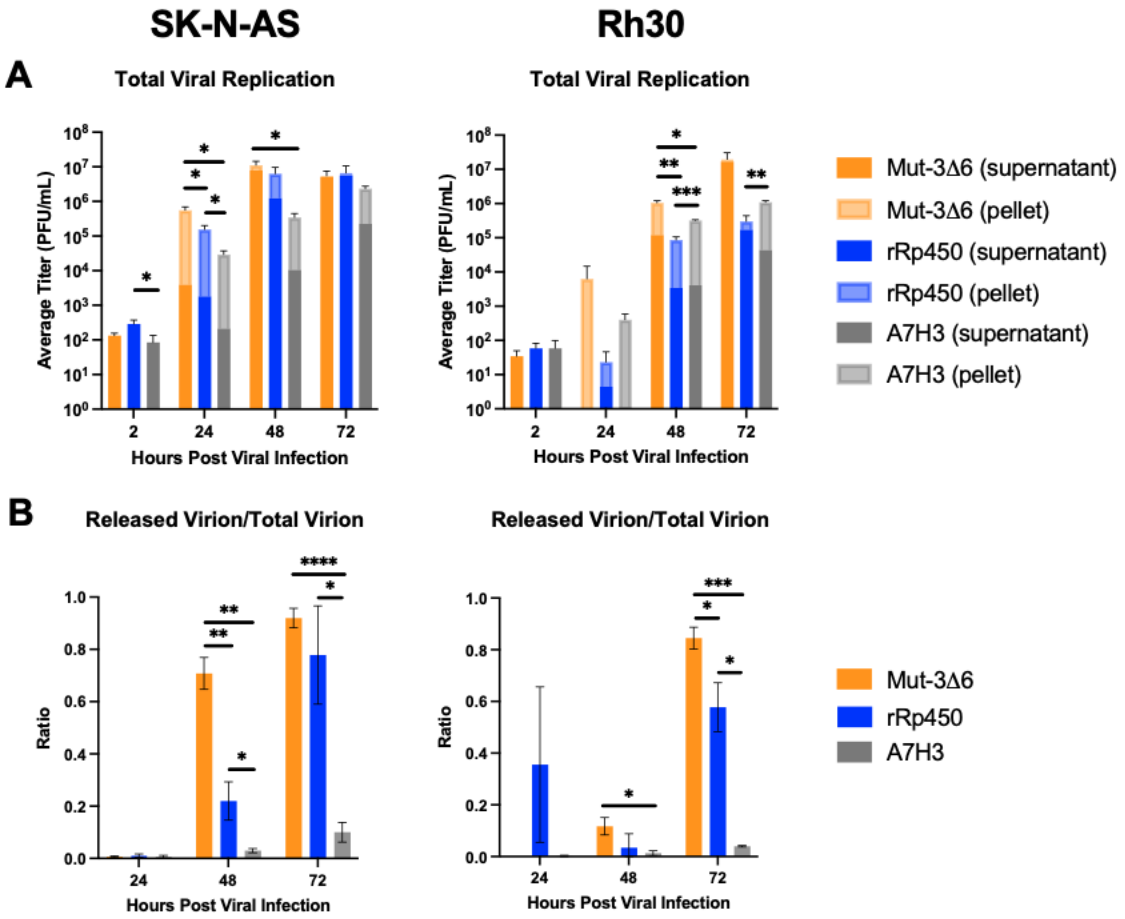

Figure 5: Viral replication in SK-N-AS and Rh30. A. Total viral replication, separated into supernatant and pellet for 24-, 48-, and 72-hours post infection, of ΔICP6 oHSVs in SK-N-AS (left) and Rh30 (right). B. Ratio of total virion released into supernatant in SK-N-AS (left) and Rh30 (right). *Note:* The majority of rRp450 samples at 24 hours had no plaques (data not shown). Due to the way in which titers are calculated, the presence of a few plaques can result in a wide range of values for samples at the same timepoint. Therefore, the ratio of rRp450 at 24 hours should be interpreted cautiously, taking the wide error bars into serious consideration.

significant differences in the replication of each oHSV (**Figure 5A**). In SK-N-AS, at 24 hours, the vast majority of virion for all oHSVs investigated was located within the cell pellet. By 48 hours, nearly 70% of Mut-3Δ6 virion was in the supernatant, and by 72 hours, nearly 90% of

Mut-3Δ6 virion was in the supernatant. In contrast, at 48 hours, only 20% of rRp450 virion was in the supernatant. The ratio of released virion compared to total virion was significantly different for Mut-3Δ6 and rRp450 at 48 hours. Furthermore, at 48 and 72 hours, both fusogenic viruses had a significantly higher proportion of released virion than non-fusogenic A7H3 (**Figure 5B**).

In Rh30, Mut-3Δ6 had a significantly higher titer than rRp450 and A7H3 at 48 hours (**Figure 5A**). At 48 hours, the ratio of released virion compared to total virion was significantly higher for Mut-3Δ6 compared to A7H3. Roughly 10% of all Mut-3Δ6 virion was in the supernatant at 48 hours, whereas <5% of rRp450 and A7H3 virion were in the supernatant. At 72 hours after infection, the proportion of Mut-3Δ6 virion in the supernatant was significantly higher than that for both rRp450 and A7H3. Roughly 85% of Mut-3Δ6 virion was in the supernatant, whereas approximately 55% of rRp450 virion and 5% of A7H3 virion, respectively, were in the supernatant (**Figure 5B**).

One day after oHSV infection, most CHP-134 cells were detached from the bottom of the well. Consequently, supernatant and pellet were not collected separately for this viral replication assay. In CHP-134, Mut-3Δ6 replicated more than its fusogenic control, rRp450, at 24, 48, and 72 hours, although not significantly. A7H3, though, replicated more than the two fusogenic viruses at 24, 48, and 72 hours. Mut-3Δ6 reached a plateau in its replication at 48 hours, whereas rRp450 and A7H3 appeared to be increasing through 72 hours (**Figure 6**).

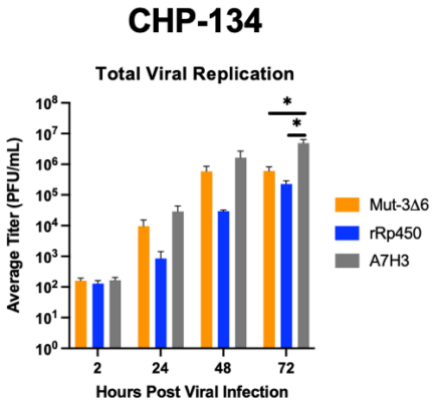

Figure 6: Viral replication in CHP-134.

Based on a holistic review of the *in vitro* data, an *in vivo* study evaluating the anti-tumor efficacy of Mut-3Δ6 in the CHP-134 tumor model was conducted. CHP-134 was chosen because Mut-3Δ6 had significantly higher potency than the other two viruses at the lowest MOIs tested (0.001, 0.01). Compared to the other cell lines, the CHP-134 MTS cytotoxicity data was the most promising in terms of cell killing reached at low MOIs that can be translated easily to the clinic. Furthermore, although the fusogenic viruses replicated less than the non-fusogenic virus in CHP-134, Mut-3Δ6 still replicated more than rRp450.

CHP-134 tumors were implanted subcutaneously in NSGS mice. Once the flank tumor reached treatable size (150-250 mm^3), the mouse was injected with PBS, rRp450 (1e7 pfu), or Mut-3Δ6 (1e7 pfu). This *in vivo* efficacy study is currently ongoing, so I will present preliminary data. I will comment on the preliminary data, but I will not formally analyze the data or draw conclusions since the study is not complete.

All male mice and three out of four female mice injected with PBS were sacrificed and two of five male mice injected with Mut-3Δ6 were sacrificed at the time of writing. All mice injected with PBS that were sacrificed at this point were sacrificed due to tumor burden exceeding endpoint criteria. One male mouse injected with Mut-3Δ6 was sacrificed due to tumor

burden, and the other male mouse injected with Mut-3Δ6 was sacrificed because he was demonstrating signs of morbidity. The tumor and organs of the male mouse that demonstrated signs of morbidity were harvested, and powder plaque assays will be performed to evaluate the presence of Mut-3Δ6 in the various tissues. None of the mice (male and female) injected with rRp450 have been sacrificed at the time of writing. All mouse weights throughout the study except for the final weight of the male mouse injected with Mut-3Δ6 that displayed signs of morbidity were within acceptable limits (>80% of weight on day of treatment). Overall, the mice injected with rRp450 exhibited greater tumor control than mice injected with Mut-3Δ6 (**Figure 7B**). One male mouse injected with rRp450 (L) has no detectable tumor and is currently considered a complete response. All other mice still alive have measurable tumors.

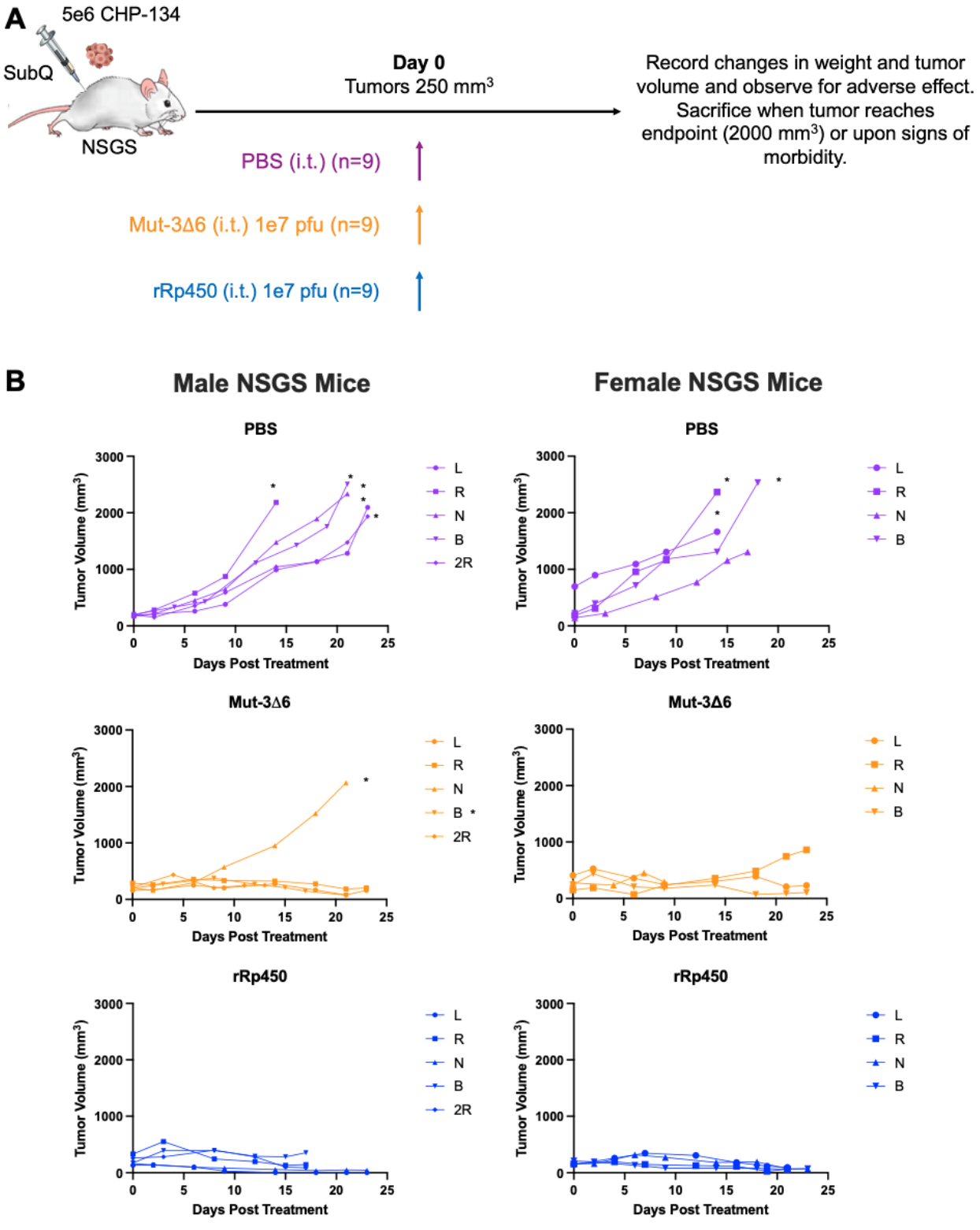
A
5e6 CHP-134
SubQ
NSGS
Day 0
Tumors 250 mm3
Record changes in weight and tumor volume and observe for adverse effect. Sacrifice when tumor reaches endpoint (2000 mm3) or upon signs of morbidity.
PBS (i.t.) (n=9)
Mut-3Δ6 (i.t.) 1e7 pfu (n=9)
rRp450 (i.t.) 1e7 pfu (n=9)
B
Male NSGS Mice
Female NSGS Mice
PBS
Mut-3Δ6
rRp450
Tumor Volume (mm3)
Days Post Treatment
L
R
N
B
2R

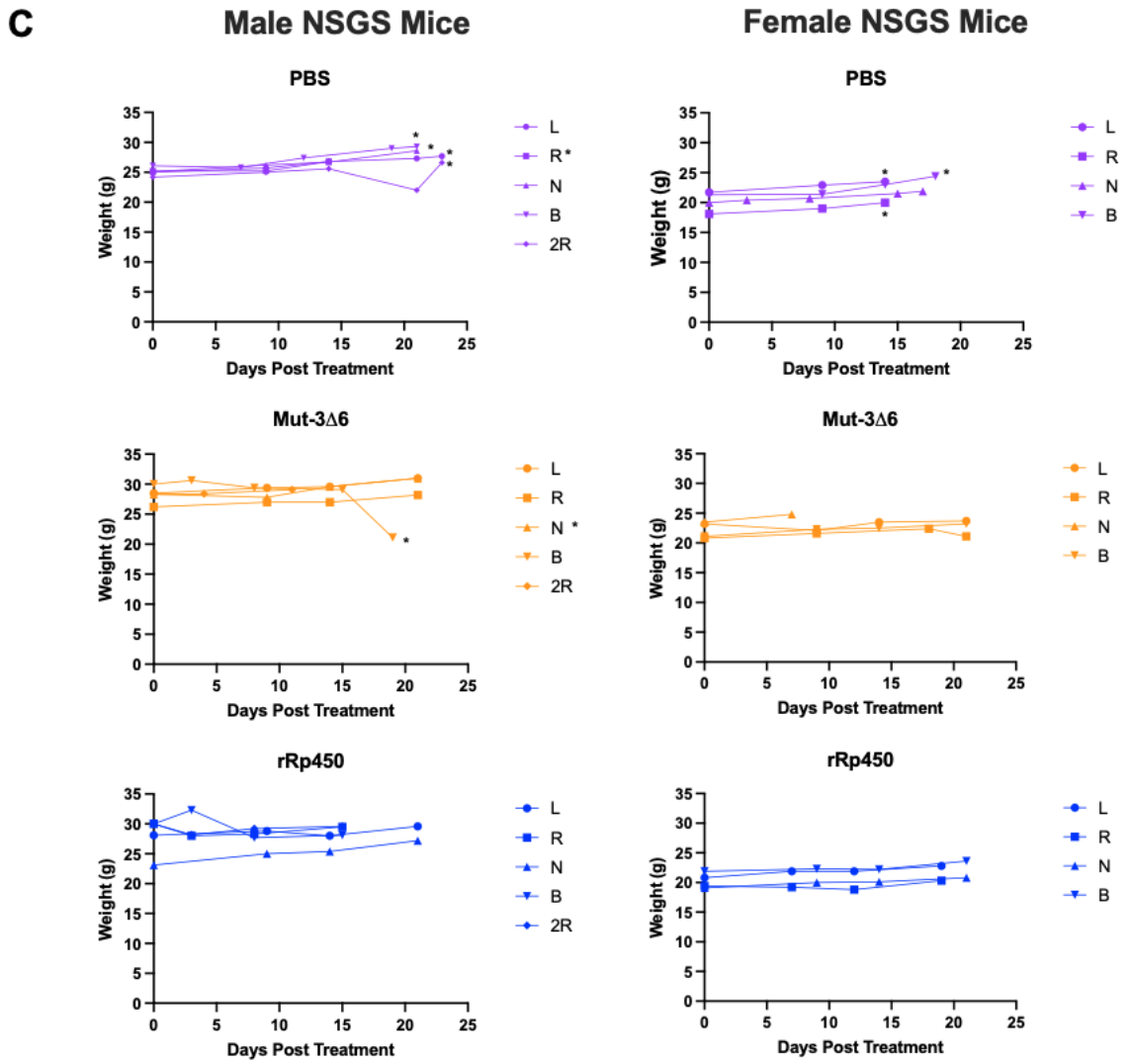

Figure 7: Preliminary Mut-3Δ6 *in vivo* anti-tumor efficacy study in the CHP-134 tumor model in NSGS mice. A. *In vivo* anti-tumor efficacy study design in NSGS mice. B. Tumor volumes of male and female mice after intratumoral treatment with PBS, rRp450, or Mut-3Δ6. C. Weights of male and female mice after intratumoral treatment with PBS, rRp450, or Mut-3Δ6.
* = mouse was sacrificed

Discussion

Mut-3Δ6 has demonstrated *in vitro* safety and *in vivo* safety. Since the safety of the novel fusogenic oHSV was established, its potency and anti-tumor efficacy was evaluated in numerous *in vitro* tumor models.

In SK-N-AS, rRp450 replicated more than Mut-3Δ6 at two hours post infection, but at 24 hours post infection, Mut-3Δ6 replicated significantly more than rRp450 and A7H3. At 48 hours, Mut-3Δ6 replicated significantly more than A7H3 but not rRp450. By 72 hours, there were no significant differences in total replication among the three viruses. When looking at replication in the supernatant and pellet separately, significant differences between Mut-3Δ6 and rRp450 emerged. At 48 hours post infection, nearly 70% of Mut-3Δ6 virion was in the supernatant as opposed to roughly 20% of rRp450 virion. Both fusogenic viruses released significantly more virion into the supernatant compared to A7H3 (non-fusogenic) at 48- and 72-hours post infection. MTS cytotoxicity data indicated Mut-3Δ6 was significantly more potent than rRp450 and A7H3 at MOI 0.001 in the high-density setting.

SK-N-AS cells infected with Mut-3Δ6 exhibited faster kinetics regarding lysis and thus virion release. There was no consistent pattern across the timepoints evaluated regarding degree of replication. However, in SK-N-AS, the ratio of released virion compared to total virion provided insight into how quickly cells infected with an oHSV were lysed. Because Mut-3Δ6 exhibited a higher release ratio at 48 and 72 hours, this indicated cell lysis occurred more quickly when cells were infected with Mut-3Δ6. The faster kinetics of cell lysis when infected with Mut-3Δ6 provided support for enhanced Mut-3Δ6 potency in SK-N-AS that was observed in MTS cytotoxicity assays (**Table 1**) because infected cells served as virion production factories that were lysed quickly, releasing infectious virion into the surrounding culture medium, thereby

promoting the infection and ultimate lysis of surrounding cells in a shorter time frame. Therefore, Mut-3Δ6 potency may be related to an enhanced rate of lysis of infected cells rather than the number of virions produced in SK-N-AS.

In Rh30, at 48 hours post infection, Mut-3Δ6 replicated significantly more than rRp450 and A7H3. Although no significant difference in total replication between rRp450 and Mut-3Δ6 was observed at 72 hours, the ratio of released virion compared to total virion was significantly greater for Mut-3Δ6 than rRp450. Rh30 MTS cytotoxicity data indicated significantly greater Mut-3Δ6 potency compared to the other two viruses at an MOI of 0.1 in the high-density setting.

In Rh30, Mut-3Δ6 had a higher total viral replication than rRp450 and A7H3 24-, 48-, and 72-hours post infection. Regarding the proportion of virion that was released into the supernatant, Rh30 cells infected with Mut-3Δ6 underwent lysis in between 48 and 72 hours, as indicated by the large increase in the ratio of Mut-3Δ6 virion found in the supernatant (~10% to ~85%). While cells infected with rRp450 and A7H3 also underwent lysis in between 48 and 72 hours, more cells infected with Mut-3Δ6 were lysed. The greater total replication of Mut-3Δ6 over time coupled with its significantly greater ratio of released virion compared to total virion indicate the potency of Mut-3Δ6 can be explained by both higher total replication and faster cell lysis. Together, these trends point towards more efficient virion production in Rh30 when infected with Mut-3Δ6.

In CHP-134, A7H3 replication exceeded Mut-3Δ6 and rRp450 replication at 24-, 48-, and 72-hours post infection. While unexpected, this observation can be rationalized. Since fusogenic viruses can spread better through syncytia, more rapid killing and lower replication can occur in some cell lines. As such, non-fusogenic viruses like A7H3 will replicate more than fusogenic viruses in some cell lines because the virus cannot spread through cell-to-cell contact. Although

A7H3 replicated more, it was not the most potent virus as measured by MTS cytotoxicity assays at MOIs of 0.001 and 0.01. On the other hand, Mut-3Δ6 was the most potent virus at MOIs of 0.001 and 0.01 in CHP-134 MTS cytotoxicity assays. Furthermore, in the CHP-134 replication assay, Mut-3Δ6 replicated more than rRp450 at 24-, 48-, and 72-hours post infection, and Mut-3Δ6 appeared to reach a plateau in replication earlier than the other two viruses, indicating faster lysis kinetics when CHP-134 cells were infected with Mut-3Δ6.

Although supernatant and pellet were not collected separately for CHP-134 because CHP-134 is a sensitive cell line, insight into replication and lysis kinetics were still gained from the total replication trends over time. CHP-134 cells infected with Mut-3Δ6 exhibited faster kinetics regarding lysis and thus virion release. Although the release ratio could not be calculated for this *in vitro* replication assay, it was conjectured that Mut-3Δ6 lysed cells more quickly than rRp450 and A7H3 since it reached a plateau in replication more quickly than the other viruses. In having faster lysis kinetics, at the same time point, it was postulated that proportionally more Mut-3Δ6 virion was found in the supernatant compared to rRp450 and A7H3. The hypothesized faster kinetics of cell lysis when infected with Mut-3Δ6 provided support for enhanced Mut-3Δ6 potency in CHP-134 that was observed in MTS cytotoxicity assays since cell survival was assayed at the same time point (three days post virus infection) for all viruses tested.

Overall, Mut-3Δ6 potency appeared to be inconsistent with the degree of replication. Total replication patterns compared to other viruses were subject to variation based on the cell line that is infected. In SK-N-AS, Mut-3Δ6 had a higher average titer than rRp450 24 hours post infection, but both fusogenic viruses replicated comparably 48- and 72 hours post infection, both having higher titers than A7H3. In Rh30, Mut-3Δ6 replicated more than rRp450 and A7H3 24-, 48-, and 72 hours post infection, and A7H3 replicated more than rRp450 at 24-, 48-, and 72

hours post infection. In SK-N-AS and Rh30, Mut-3Δ6 had a higher ratio of released virion than rRp450 and A7H3 at 48- and 72 hours post infection. In CHP-134, A7H3 replicated more than both fusogenic viruses at 24-, 48-, and 72 hours post infection, but Mut-3Δ6 nonetheless replicated more than rRp450 at the same timepoints. Also, Mut-3Δ6 appeared to plateau in its average titer at 48 hours post infection whereas rRp450 and A7H3 were still increasing in average titer through 72 hours post infection in CHP-134. There may be cell-line specific mechanisms at play that result in these interesting patterns, but in general, Mut-3Δ6 replication exceeded rRp450 replication for at least one timepoint across the cell lines tested. Additionally, the data indicated Mut-3Δ6 potency can be explained by Mut-3Δ6 infection leading to faster lysis of infected cells compared to the other viruses investigated, resulting in greater cell killing.

Since only three replicates were used for each timepoint in the viral replication assays, the small sample limits the statistical power to deem the differences in the titers to be significant. To address statistical limitations, in future studies, experiments will be designed to have more replicates to increase the power of the significance test. Additionally, plaque assays were performed by creating log-fold serial dilutions of the samples containing virus. Some samples were countable at different dilutions, and since the titer calculation involves multiplying by the dilution factor, the log-fold differences that can emerge from the nature of the assay and its analysis likely contribute to the large standard deviations of the samples. These large standard deviations also limit the statistical power, which explains why some of the titers look significantly different on the graph but do not have a small enough p value to be significant.

Mut-3Δ6 is currently being investigated in an *in vivo* CHP-134 tumor model. Although the study is not complete, rRp450 has demonstrated greater anti-tumor efficacy than Mut-3Δ6 to date, which is unexpected based on the *in vitro* data. Since tumors were injected with 1e7 pfu of

virus, it was hypothesized that Mut-3Δ6 would shrink tumors more than rRp450 and potentially facilitate cures based on the *in vitro* data. At this point, the only cure has occurred in a male mouse injected with rRp450. One possible explanation of this observation is the amount of virus injected was not 1e7 pfu. Since the tumors reached treatable sizes at different times, it was logistically very challenging to confirm the amount of virus injected. The proper way to confirm the amount of virus injected is to do a back titer plaque assay after each injection of virus. To do a back titer plaque assay, Vero cells must be plated one day prior to injection. Since it was hard to predict when tumors would reach a treatable size, back titer plaque assays were not performed. If mice injected with rRp450 were injected with more than 1e7 pfu and/or mice injected with Mut-3Δ6 were injected with less than 1e7 pfu, then it is plausible that rRp450 would exhibit greater anti-tumor efficacy than Mut-3Δ6.

Another possible explanation of the *in vivo* efficacy differences lies within the tumor microenvironment. The *in vivo* study was conducted in immunodeficient mice, so there were likely few functional immune cells in the tumor microenvironment. However, other components of the tumor microenvironment, such as the extracellular matrix, may have provided barriers to efficient Mut-3Δ6 spread. The extracellular matrix forms an "interlocked meshwork of secreted proteins [that] presents a physical barrier that interferes with efficient dispersal of therapeutics within the solid tumor" (Wojton & Kaur, 2010). Therefore, the spread of Mut-3Δ6 may have been hindered by the extracellular matrix. Consequently, the gigantic fusogenic phenotype of Mut-3Δ6 may not have been fully realized in the *in vivo* CHP-134 tumors because of the physical barricade presented by the extracellular matrix, which may explain why Mut-3Δ6 has been less efficacious than rRp450 to date in controlling tumor growth.

It is important to recognize that the *in vivo* efficacy study is not complete, and my conjecture is based on preliminary data. A finalized analysis will be performed once the study is complete.

Evaluating the degree to which different tumor models respond to oHSV treatment *in vitro* and *in vivo* aids in the identification of cancers for which oHSV treatment is promising, which may lead to clinical trials that shape the standard of care for cancer patients in the future. It can also begin to elucidate the mechanisms behind tumor models bearing oHSV resistance, one of the most prevailing challenges in the discipline. Although *in vivo* efficacy conclusions cannot be made yet, with demonstrated *in vitro* safety and potency and *in vivo* safety, this investigation of Mut-3Δ6 has provided valuable insight into its potential as a cancer therapeutic.

Materials and Methods

Cell Culture: Cells were cultured in their designated complete medium and incubated at 37°C in 5% CO_2. All cells were tested for Mycoplasma contamination and confirmed to be negative.

Virus Preparation: Fifteen to thirty plates of BHK were cultured in E10. Plates were infected with virus from a prior preparation. When most cells were infected, the plates were scraped, and the cells and supernatant were harvested and stored at -80°C. The tubes were spun down at 4,000 rpm for 20 minutes, and the supernatant was decanted and filtered through a 0.8 μM filter. The filtrate was kept on ice. The pellets were resuspended in 10 to 20 mL total of cold PBS. The resuspended pellets were freeze/thawed three times and then spun down at 4,000 rpm for 20 minutes. The supernatant was decanted and filtered through the same 0.8 μM filter. The filtrate was centrifuged at 13,000 rpm for two hours at 4°C. After high-speed centrifugation, the supernatant was decanted, and the viral pellet was resuspended in viral preparation medium (15% glycerol in plain EMEM). Viruses were titered by plaque assay.

MTS Cytotoxicity Assays: MTS cytotoxicity assays were performed to evaluate cell survival after infection with the three ΔICP6 oHSVs studied. Cells were seeded in their designated complete culture medium at 5,000 (low density) or 20,000 (high density) cells per well in a 96-well plate. The density was visually confirmed under a microscope, and the cells were incubated at 37°C overnight. The next day, cells were infected in hexaplicate at multiplicity of infection (MOI; ratio of virus added to designated number of cells) of 0.001, 0.01, 0.1, 1, and 10 with virus diluted in complete media (usually R10). Three days later, 20 μL MTS/PMS reagent was added to each well,

and the plate was read three hours later at 490 nm. Virus titers were confirmed using a back titer plaque assay (50 μL virus + 100 μL plain EMEM).

To evaluate the cytotoxicity of each virus, the average absorbance at each MOI was computed and expressed as a percentage of the average absorbance of the control (cells and media only). The standard deviation of the absorbances at each MOI was computed and expressed as a percentage of the average absorbance of the control. Unpaired t-tests with Welch's correction were performed to determine if the average cell survival varied based on which virus was used to infect the cells. Unpaired t-tests were used because the samples were independent. Welch's correction was applied since the standard deviations were not the same for both samples that were analyzed in each unpaired t-test.

Viral Replication Assays: Cells were seeded in their designated complete culture medium at 2e5 cells per well in a 12-well plate and incubated overnight. The next day, the media was aspirated, and human lines (SK-N-AS, Rh30, CHP-134) were infected with 500 μL of rRp450, Mut-3Δ6, and A7H3 individually at MOI 0.01. Plates were rocked every 15-20 minutes. After two hours, the supernatant was aspirated from all wells. Each well was then gently washed with 1 mL room temperature PBS. CHP-134 was not washed with PBS since cells can be lifted easily from the well. Upon aspiration of PBS, 1 mL designated complete culture medium was added to each well. The 2-hour timepoint sample was collected by scraping the wells with a pipet tip. 1 mL of each sample was transferred to an Eppendorf tube. The same collection process was performed at 24, 48, and 72 hours after infection, and supernatant and pellet were collected separately for these time points for Rh30 and SK-N-AS. Samples for CHP-134 were not collected separately because most cells

were detached at 24 hours. Samples were stored at -80°C. Plaque assays were performed to titer the samples.

Plaque Assays: The amount of virus present in each sample was analyzed through plaque assays. For the plaque assays, Vero cells were plated at 2-3e6 cells per plate in 6-well or 12-well plates in E10 and incubated overnight. Samples were freeze/thawed three times total, and each sample was used to make serial dilutions of the virus in plain EMEM. If titering a virus preparation, the virus stock was used to make serial dilutions in plain EMEM. After aspirating the media from each well, 100 μL of plain EMEM was added, and 100 μL of each virus dilution was later added to infect the cells. Plates were rocked every 15-20 minutes. After a 90-minute incubation, overlay was added to each well. Three days later, the plates were stained with Crystal Violet. After staining for 20-30 minutes, the stain was washed away. Plaques were counted and averaged in triplicate for the countable dilution to calculate the titer.

For samples separated into supernatant and pellet (SK-N-AS, Rh30), the titer of the supernatant and the titer of the pellet were calculated individually. For each timepoint, there were three samples, which consisted of supernatant and pellet. The total titer for each sample was calculated by adding the titer of the supernatant and pellet together. Then, the average of the total titers for samples of the same timepoint was calculated (n = 3). The standard deviation of the average titer was also calculated for each timepoint. Furthermore, the ratio of released virion compared to total virion present in the sample was calculated for samples separated into supernatant and pellet by dividing the titer of the supernatant for the sample by the total titer of the sample. The average ratio and standard deviation were calculated for each timepoint (n = 3). For CHP-134, supernatant

and pellet were not collected separately. Therefore, total viral replication was evaluated. The titer for each sample at each timepoint was calculated. Then, the average of the titers for samples of the same timepoint was calculated (n = 3). The standard deviation of the average titer was also calculated for each timepoint. Unpaired t-tests with Welch's correction were performed to determine if the average titer varied based on which virus was used to infect the cells at each timepoint. Unpaired t-tests were used because the samples were independent. Welch's correction was applied since the standard deviations were not the same for both samples that were analyzed in each unpaired t-test.

in vivo Efficacy Study: 5e6 CHP-134 cells in 33% Matrigel were injected subcutaneously in NSGS male (n = 15) and female (n = 12) mice that were 5- to 6-weeks old. Mice were monitored for tumor take, and when tumors reached a treatable size (~150-250 mm^3), 1e7 pfu of rRp450 (in 100 μL cold PBS), 1e7 pfu of Mut-3Δ6 (in 100 μL cold PBS), or 100 μL cold PBS was injected intratumorally. Mice were weighed weekly, and tumor volumes were measured biweekly using calipers. Tumor was calculated using the following formula: $(length \times width^2) \times \pi/6$. Mice were also monitored for signs of morbidity. When a tumor reached endpoint criteria (2000 mm^3 total volume or tumor length greater than 2 cm) or the mouse exhibited signs of morbidity, the mouse was sacrificed humanely. This study was conducted under approved IACUC protocol AR12-00074.

Statistical Methods: Unpaired t-tests with Welch's correction were performed in GraphPad Prism 9 for macOS (GraphPad Software, La Jolla, CA, USA).

References

Agelidis AM, Shukla D. Cell entry mechanisms of HSV: what we have learned in recent years. Future Virol. 2015 Oct 1;10(10):1145-1154. doi: 10.2217/fvl.15.85.

Bilsland AE, Spiliopoulou P, Evans TRJ. Virotherapy: cancer gene therapy at last? *F1000Research*. 2016;5:F1000 Faculty Rev–2105. doi:https://doi.org/10.12688/f1000research.8211.1

Bolovan CA, Sawtell NM, Thompson RL. ICP34.5 mutants of herpes simplex virus type 1 strain 17syn+ are attenuated for neurovirulence in mice and for replication in confluent primary mouse embryo cell cultures. *Journal of Virology*. 1994;68(1):48-55. doi:https://doi.org/10.1128/JVI.68.1.48-55.1994

Chase M, Chung RY, Chiocca EA. An oncolytic viral mutant that delivers the CYP2B1 transgene and augments cyclophosphamide chemotherapy. *Nature Biotechnology*. 1998;16(5):444-448. doi:https://doi.org/10.1038/nbt0598-444

Cripe TP, Chen CY, Denton NL, et al. Pediatric cancer gone viral. Part I: strategies for utilizing oncolytic herpes simplex virus-1 in children. *Molecular Therapy - Oncolytics*. 2015;2. doi:https://doi.org/10.1038/mto.2015.15

Cunningham RM, Walton MA, Carter PM. The Major Causes of Death in Children and Adolescents in the United States. *New England Journal of Medicine*. 2018;379(25):2468-2475. doi:https://doi.org/10.1056/nejmsr1804754

Ennis, M, Russell, S, Dingli, D. Fusion Versus Lysis: Non-Fusogenic Measles Viruses as Oncolytic Agents. *Molecular Therapy.* 2009;17(Supplement 1): S3. https://doi.org/10.1016/S1525-0016(16)38365-4

Groeneveldt C, van den Ende J, van Montfoort N. Preexisting immunity: Barrier or bridge to effective oncolytic virus therapy? *Cytokine & Growth Factor Reviews*. 2023;70:1-12. doi:https://doi.org/10.1016/j.cytogfr.2023.01.002

Kline N, Sevier N. Solid Tumors in Children. *Journal of Pediatric Nursing*. 2003;18(2). doi:https://doi.org/10.1053/jpdn.2003.12

Krabbe T, Altomonte J. Fusogenic Viruses in Oncolytic Immunotherapy. *Cancers*. 2018;10(7):216. doi:https://doi.org/10.3390/cancers10070216

Kuhn I, Harden P, Bauzon M, et al. Directed Evolution Generates a Novel Oncolytic Virus for the Treatment of Colon Cancer. Jin DY, ed. *PLoS ONE*. 2008;3(6):e2409. doi:https://doi.org/10.1371/journal.pone.0002409

Kukhanova MK, Korovina AN, Kochetkov SN. Human herpes simplex virus: Life cycle and development of inhibitors. *Biochemistry (Moscow)*. 2014;79(13):1635-1652. doi:https://doi.org/10.1134/s0006297914130124

Lehman IR, Boehmer PE. Replication of Herpes Simplex Virus DNA. *Journal of Biological Chemistry*. 1999;274(40):28059-28062. doi:https://doi.org/10.1074/jbc.274.40.28059

Nguyen HM, Guz-Montgomery K, Saha D. Oncolytic Virus Encoding a Master Pro-Inflammatory Cytokine Interleukin 12 in Cancer Immunotherapy. *Cells*. 2020;9(2):400. doi:https://doi.org/10.3390/cells9020400

Nguyen HM, Saha D. The Current State of Oncolytic Herpes Simplex Virus for Glioblastoma Treatment. *Oncolytic Virotherapy*. 2021;10:1-27. doi:https://doi.org/10.2147/ov.s268426

Peters C, Rabkin SD. Designing herpes viruses as oncolytics. *Molecular Therapy - Oncolytics*. 2015;2:15010. doi:https://doi.org/10.1038/mto.2015.10

Roizman, B, Knipe, DM and Whitley, RJ. Herpes simplex viruses. In: Knipe DM and Howley PM (eds). *Fields Virology*. Lippincott Williams &Wilkins, Philadelphia, 2013. pp 1823–1897.

Varghese, S., Rabkin, S. Oncolytic herpes simplex virus vectors for cancer virotherapy. *Cancer Gene Ther* 9, 967–978 (2002). https://doi.org/10.1038/sj.cgt.7700537

Wang PY, Swain HM, Kunkler AL, et al. Neuroblastomas Vary Widely in Their Sensitivities to Herpes Simplex Virotherapy Unrelated to Virus Receptors and Susceptibility. *Gene therapy*. 2016;23(2):135-143. doi:https://doi.org/10.1038/gt.2015.105

Weller SK, Coen DM. Herpes simplex viruses: mechanisms of DNA replication. Cold Spring Harb Perspect Biol. 2012 Sep 1;4(9):a013011. doi: 10.1101/cshperspect.a013011.

Wojton J, Kaur B. Impact of tumor microenvironment on oncolytic viral therapy. *Cytokine & Growth Factor Reviews*. 2010;21(2-3):127-134. doi:https://doi.org/10.1016/j.cytogfr.2010.02.014

Xu F, Schillinger JA, Sternberg MR, Johnson RE, Lee FK, Nahmias AJ, Markowitz LE. Seroprevalence and coinfection with herpes simplex virus type 1 and type 2 in the United States, 1988-1994. J Infect Dis. 2002 Apr 15;185(8):1019-24. doi: 10.1086/340041.